

CONDICIONES EXTENDIDAS DE SINCRONIZACIÓN DE DOS MAPAS LOGÍSTICOS ACOPLADOS SYNCHRONIZATION EXTENDED CONDITIONS OF TWO COUPLED LOGISTIC MAPS

R. O. E. BUSTOS ESPINOZA[†] & G. M. RAMÍREZ ÁVILA[‡]

Instituto de Investigaciones Físicas, Universidad Mayor de San Andrés
Campus Universitario, c. 27 Cota-Cota, Casilla de Correos 8635
La Paz - Bolivia

(Recibido 10 de agosto de 2020; aceptado 15 de septiembre de 2020)

RESUMEN

Se analizan las regiones de sincronización de dos mapas logísticos acoplados difusivamente en un amplio plano de parámetros. Se encontraron nuevas estructuras bien definidas que amplifican la caracterización de dos osciladores móviles. Debido a su simplicidad y a su rico comportamiento dinámico, los mapas logísticos acoplados nos permiten estudiar diferentes tipos de sincronización. Nos enfocamos específicamente en la sincronización en fase caracterizándola mediante periodicidades que se presentan simétricamente en el plano de parámetros. Lo anterior, nos permite distinguir claramente entre regiones con comportamiento regular o caótico. Finalmente, se indican posibles aplicaciones de este tipo de sistemas.

Código(s) PACS: 05.45.Xt, 05.45.Pq, 05.45.-a

Descriptores: Sincronización, caos — sistemas caóticos — dinámica no lineal.

ABSTRACT

We analyze the synchronization regions of two diffusively coupled logistic maps in an ample parameter plane where we found new and well-defined structures of synchrony that allow us to amplify the characterization of two motile oscillators. Due to their simplicity and rich dynamical behavior, the coupled logistic maps enable us to study different kinds of synchronization. We focus specifically on phase synchronization characterizing it by periodicities that symmetrically pervades the parameter plane. A clear distinction is found between the above mentioned synchronous regions from those exhibiting chaotic behavior. Finally, we point out some possible applications of this kind of system.

Subject headings: Synchronization, chaos — chaotic systems — nonlinear dynamics.

1. INTRODUCTION

The synchronization phenomena, so abundant in nature, and extensively studied in a wide variety of systems, from physics to social sciences, is defined by Pikovsky et al. (2001) as an adjustment of rhythms of self-sustained oscillators due to their interactions. Several works have been devoted to study synchronous behavior in different kind of oscillators, for instance, in electronically-implemented systems, such as the paradigmatic chaotic circuit proposed by Chua and introduced by Matsumoto (1984). Coupled Chua's circuits give rise to chaotic synchronization firstly formulated intuitively by Tang et al. (1983), and demonstrated afterwards by Chua (1993). Other interesting circuits exhibiting synchronization are the light controlled oscillators introduced by Ramírez-Ávila et al. (2003), and characterized by their pulsatile coupling; and also that conceived by L'Her et al. (2016) for studying coupled

logistic maps. It is worthy to mention the oscillators introduced by Kuramoto & Nishikawa (1987) which became an example for excellence for studying synchronization in different network configurations in many contexts, including power-grids described by Schultz et al. (2014), and in mobile agents studied by Fujiwara et al. (2011). The omnipresence of synchronization in nature makes that this phenomenon acquires an essential role in science due to their universal feature that is understood within the nonlinear dynamics conceptual framework as expounded by Fujisaka & Yamada (1983). The study of synchronization using maps was started with the work of Yamada & Fujisaka (1983). Some other interesting systems described by maps exhibit synchronization such as in neurons described by Sun & Cao (2016), Calderón de la Barca, & Ramírez-Ávila (2017) and Iglesias & Ramírez-Ávila (2019), and even in social systems which are studied through the relationship between synchronization and consensus as stated in the edited book of Kocarev (2013), and analyzed in terms of discrete models by Subieta-

[†]<http://www.fiumsa.edu.bo/docentes/rbustos/>

[‡]<http://www.fiumsa.edu.bo/docentes/mramirez/>

Frías & Ramírez-Ávila (2017). Transients or synchronization time, plays also an important role in the description of synchronization as pointed out by Ramírez-Ávila et al. (2006), where they study synchronization regions and transients in locally coupled oscillators in linear and ring configurations.

In this work, we describe a huge region of the parameter plane of a systems composed of two coupled logistic maps, where the dynamical behavior allowed us to describe the synchronous behavior of the system according to the coupling strength, and the difference between the oscillators. The description in terms of periodicities gives an insight of the dynamical behavior of such a system. This paper is organized as follows: the logistic map and its features are set forth in Sect. 2, the model for two coupled maps is presented in Sect. 3, where we focus on the types of coupling, the definition of the synchronization ability factor, the synchronization regions and some other important remarks. The results are presented in Sect. 4 emphasizing in the aspects related to periodicities and the possibility of varying coupling in relationship with mobile oscillators. Finally, in Sect. 5, we give conclusions and some perspectives.

2. THE LOGISTIC MAP AND ITS FEATURES

The logistic map is represented by a recurrent equation based on a model proposed by Verhulst (1838). This model describes population dynamics taking into account aspects like birth and death rate. This map was formulated by May (1976) who realized about the complicated dynamics exhibited by this very simple system including chaotic behavior.

This map has been used in many different disciplines and situations going from studies on competitive models, developed by Burgoa & Nogales (2001) to the emergence of coherent motion as studied by García-Cantú et al. (2011), and the spatiotemporal intermittency in coupled maps lattices described by Kaneko (1985), and Chaté & Manneville (1988). On the other hand, due to their simplicity and robustness as chaos generator, coupled logistic maps have been extensively used to describe synchronization in different scenarios as for instance with delayed coupling as studied by Masoller et al. (2001). For the above-mentioned reasons, we chose as a model for the dynamics of each of the oscillators a logistic map given by:

$$D_{n+1} = \mu D_n (1 - D_n), \quad (1)$$

where D_n is a number between zero and one that represents the dynamics of the oscillator. D_0 represents the initial condition; μ is the control parameter, a positive number whose value determines the dynamical behavior of the map, and n plays the role of time, as explained in Bustos-Espinoza & Ramírez-Ávila (2012).

2.1. Main hypothesis

We work with two coupled oscillators, considering the following simplifying assumptions concerning their dynamics:

- The coupled oscillators constitute an isolated system.
- Each oscillator follows a logistic map dynamics.
- The oscillators cannot collide.
- We assume that the oscillators interact in two modes: maintaining a fixed distance between them or not (see Sect. 3)

3. MODEL

Intending to study the synchronization of two motile or static oscillators, we consider the instantaneous coupling between two logistic maps whose dynamical equations are:

$$\begin{aligned} D_{n+1}^{(1)} &= \mu^{(1)} D_n^{(1)} (1 - D_n^{(1)}) + \beta_{12} (D_n^{(2)} - D_n^{(1)}) \\ D_{n+1}^{(2)} &= \mu^{(2)} D_n^{(2)} (1 - D_n^{(2)}) + \beta_{21} (D_n^{(1)} - D_n^{(2)}) \end{aligned}, \quad (2)$$

where superscripts identify the oscillators and subscripts represent the temporal evolution, and β represents the coupling strength between oscillators. Assuming the coupling symmetry: $\beta_{12} = \beta_{21} = \beta$. We consider the following cases:

- Constant coupling ($\beta = \text{const}$):
 β constant means that oscillators do not move and the coupling strength does not change.

$$\beta = \beta_{12} = \beta_{21} = \text{constant} \quad . \quad (3)$$

- Distance dependent coupling ($\beta \neq \text{const}$):
 $\beta \neq \text{const}$, means that oscillators can move. We proposed that the coupling strength varies with the inverse of the square of the Euclidean distance ρ , between their spatial positions, $(x_n^{(i)}, y_n^{(i)}, z_n^{(i)})$, of the oscillators:

$$\begin{aligned} \beta &\propto \rho^{-2} \\ \rho_n &= \sqrt{(x_n^{(2)} - x_n^{(1)})^2 + (y_n^{(2)} - y_n^{(1)})^2 + (z_n^{(2)} - z_n^{(1)})^2} \end{aligned} \quad . \quad (4)$$

3.1. Existence Conditions

Taking into account that D_n must be defined in the interval $[0, 1]$, and in order to avoid values out of range, we need to impose the conditions:

$$\begin{aligned} \text{if } D_n &\geq 1 &\Rightarrow D_n &= 1 \\ \text{if } D_n &\leq 0 &\Rightarrow D_n &= 0 \end{aligned} \quad .$$

3.2. Abstract Vector

In order to study the oscillators' dynamics, we define the following n -dimensional abstract vector, \vec{V} ,

$$\vec{V}_n^{(i)} = f(D_n^{(i)}, \rho_n) \quad , \quad i = 1, 2 \quad , \quad (5)$$

where $D_n^{(i)}$ represents the i -th oscillator dynamics and ρ_n the Euclidean distance with respect to other oscillator. In this manner, we consider that each oscillator will be described by this new mathematical definition.

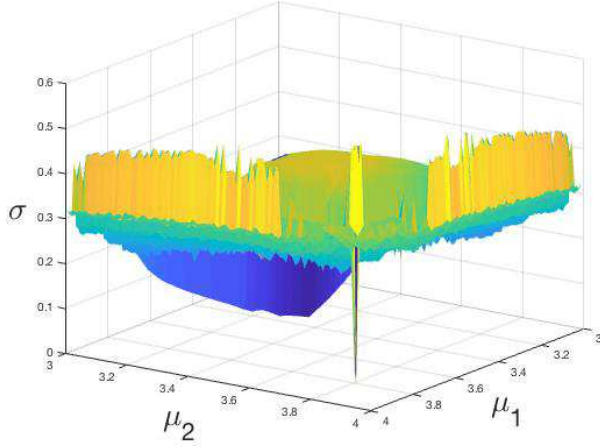


FIG. 1.— (Color online) Synchronizability factor σ_n in terms of the parameters μ_1 and μ_2 , after $n = 10^6$ time steps, for two coupled logistic maps defined in the interval $[3, 4]$ and being $\beta = 0.0029$.

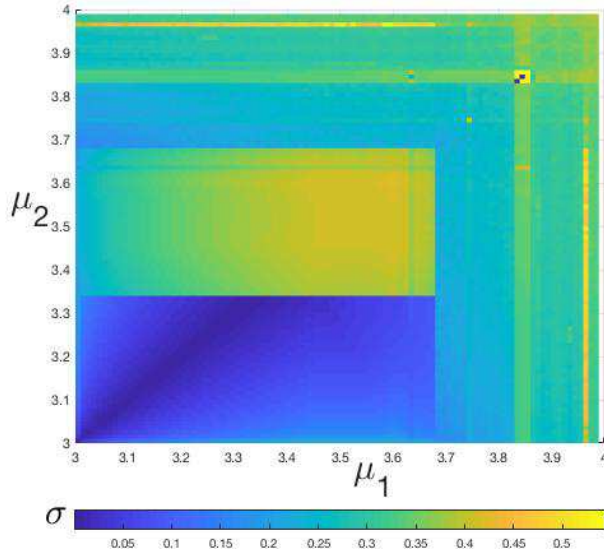


FIG. 2.— (Color online) Parameter plane (μ_1, μ_2) , in terms of the synchrony factor σ_n whose values are related to the color bar.

3.3. Synchronizability Factor

In order to quantify the general synchronization between two or more oscillators we define the *synchronizability factor* as:

$$\sigma_n^{i,j} = \frac{1}{\binom{N}{2}} \sum_{j=1}^{N-1} \sum_{k>j}^N \left| D_n^{(i)} - D_n^{(j)} \right|, \quad (6)$$

where in the case of two oscillators, as used by Bustos-Espinoza & Ramírez-Ávila (2012):

$$\sigma_n^{1,2} = \left| D_n^{(1)} - D_n^{(2)} \right|. \quad (7)$$

There are many works dedicated to synchronization on coupled maps that use a synchronization factor as the indicator to characterize synchronization, e.g., several authors used the variance as such an indicator, i.e., $\sigma^2 = \frac{1}{N} \left\langle \sum_i [x_i(t) - \langle x \rangle]^2 \right\rangle_t \rightarrow 0$ to ana-

lyze coupled chaotic maps. Thus, Lind et al. (2004) adopt this indicator to study the coherence in scale-free networks; Masoller & Martí (2005) employ the variance to characterize the synchronous behavior of an array with random delays in the maps' dynamics; Lind et al. (2006) use this indicator in networks with different topologies and considering delayed couplings. In this work, we characterize synchronization using Eq. (7) when $\sigma_n \rightarrow 0$ for describing complete synchronization, in the same line of the usage of the variance as an indicator. Besides, we also consider the periodical oscillating behavior of σ_n as a manner to characterize phase-synchronization.

3.4. Cases Studied

We considered three synchronous situations: *complete synchronization* and *antisynchronization* means a synchronization in phase and amplitude, while *phase synchronization* means a periodicity value for each synchrony factor considered. Thus, we define each case as a behavior of the synchronizability factor,

- Complete synchronization: ($\sigma_n \rightarrow 0$)
- Complete Antisynchronization: ($\sigma_n \rightarrow 1$)
- Phase synchronization: ($\sigma_n \rightarrow \text{oscillant}$)

3.5. Spatial Positions and Synchronization

Following our model, each oscillator can keep a fixed distance as long as we get a synchronization factor threshold, $\sigma_n^{\text{threshold}}$, indicating that the system tends toward complete synchronization; in that case, the oscillators turn on synchronized. We can express that fact with the following expression:

$$\begin{aligned} \text{if } \sigma_n \geq \sigma_n^{\text{threshold}} &\Rightarrow \\ \left(x_{n+1}^{(i)}, y_{n+1}^{(i)}, z_{n+1}^{(i)} \right) &= \left(x_n^{(i)} + \Delta x, y_n^{(i)} + \Delta y, z_n^{(i)} + \Delta z \right) \\ \text{if } \sigma_n < \sigma_n^{\text{threshold}} &\Rightarrow \\ \left(x_{n+1}^{(i)}, y_{n+1}^{(i)}, z_{n+1}^{(i)} \right) &= \left(x_n^{(i)}, y_n^{(i)}, z_n^{(i)} \right), \end{aligned} \quad (8)$$

where Δx , Δy and Δz , are small random displacements in the x , y and z directions respectively, following a Gaussian distribution.

3.6. Noncollisional Condition

In order to avoid collisions between oscillators once we randomly generate their initial positions, we introduce the condition:

$$\begin{aligned} \text{if } d_n \leq d_{\text{threshold}} &\Rightarrow \\ \left(x_{n+1}^{(i)}, y_{n+1}^{(i)}, z_{n+1}^{(i)} \right) &= \left(x_n^{(i)} + \Delta x, y_n^{(i)} + \Delta y, z_n^{(i)} + \Delta z \right) \\ \wedge d_{n+1} > d_n &, \end{aligned} \quad (9)$$

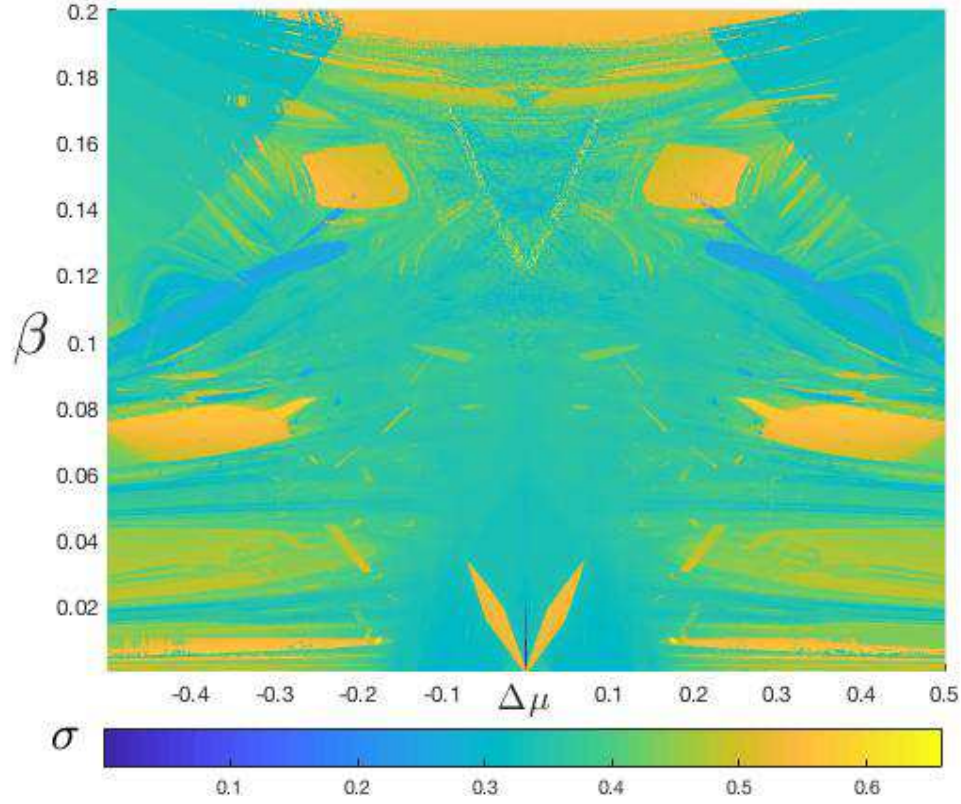


FIG. 3.— (Color online) Synchronization regions, obtained with $\mu^{(1)} = \mu^{(2)} = 3.83$, in the plane coupling strength (β) vs. parameter mismatch ($\Delta\mu$) and described in terms of the synchronizability, σ whose values are represented in the color bar, similar to that used in Fig. 2. The central down part was reported by Bustos-Espinoza & Ramírez-Ávila (2016).

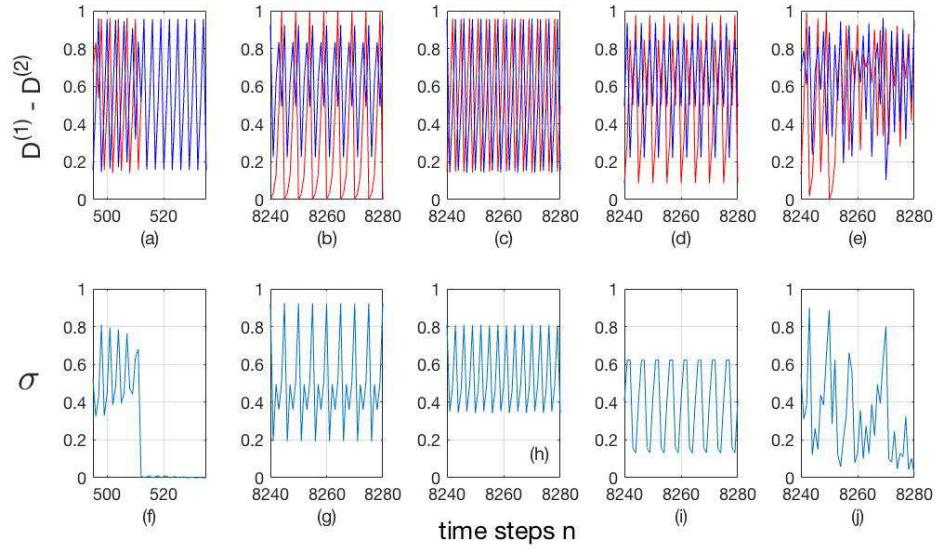


FIG. 4.— (Color online) (a)–(e) Time series of variables $D^{(1)}$ (blue) and $D^{(2)}$ (red), and (f)–(j) synchronizability, σ : (a) and (f): $\Delta\mu = 0.0000$, $\beta = 0.0064$, *complete synchronization* ($\sigma \rightarrow 0$); (b) and (g): $\Delta\mu = 0.2045$, $\beta = 0.0342$, *phase synchronization* ($\sigma_P = 5$); (c) and (h): $\Delta\mu = 0.0220$, $\beta = 0.0128$, *phase synchronization* ($\sigma_P = 6$); (d) and (i): $\Delta\mu = 0.0695$, $\beta = 0.0128$, *phase synchronization* ($\sigma_P = 10$); (e) and (j): $\Delta\mu = 0.0685$, $\beta = 0.0545$, *chaos* ($\sigma_P \rightarrow \infty$).

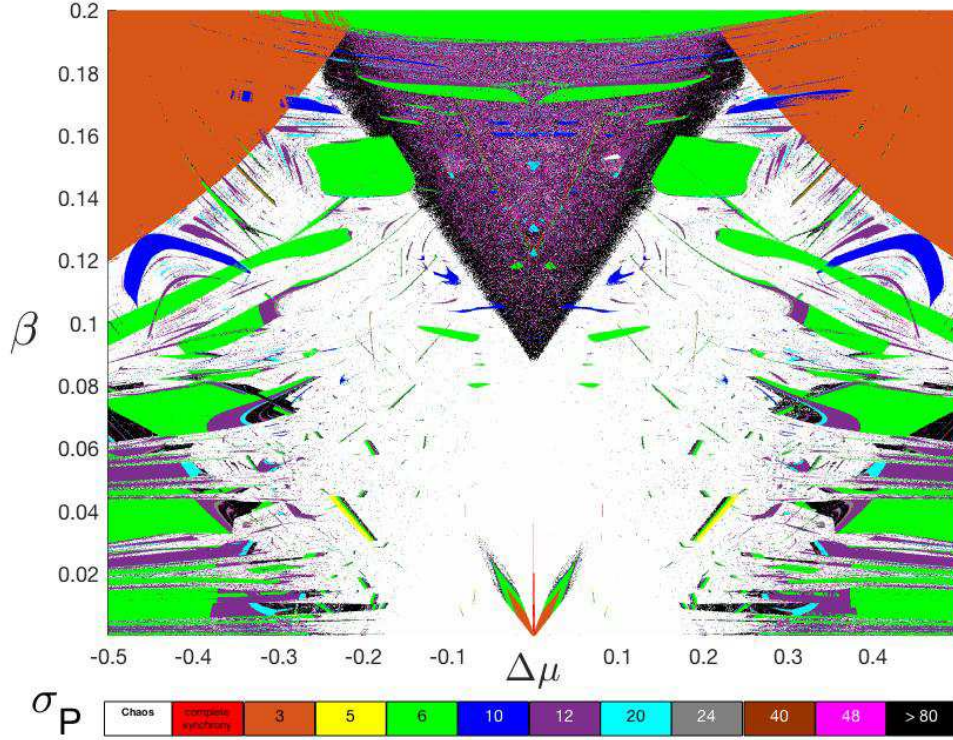


FIG. 5.— (Color online) Phase diagram: $\Delta\mu$ vs. β in terms of σ_P . The horizontal color bar represents the main periodicities appearing in the synchronization regions and also the situation of non-synchronization (white=chaos). The darkness regions (black color) means periods greater than 80. It is important to underline a integer sequence of periods found: 3, 5, 6, 10, 12, 20, 24, 40, 48, 80,... Bustos-Espinoza & Ramirez-Ávila (2016) reported the central down part.

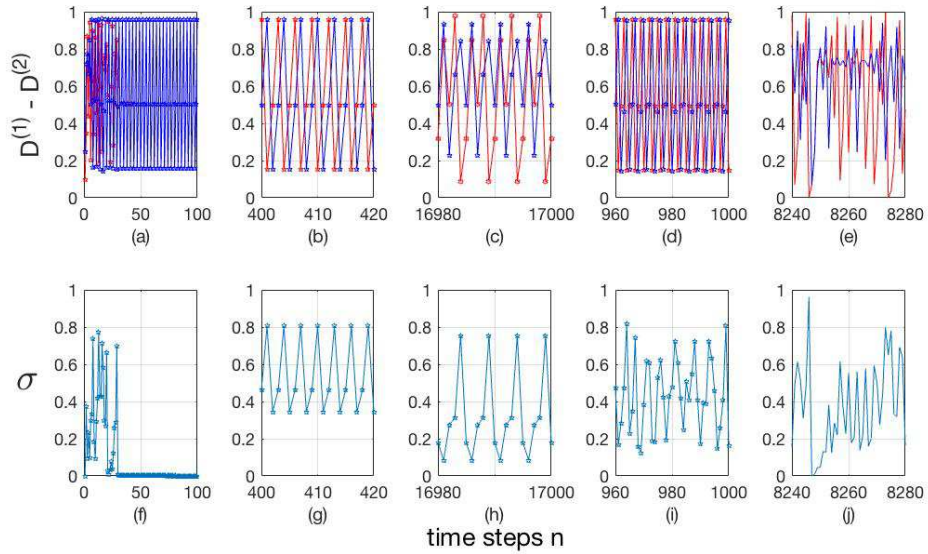


FIG. 6.— (Color online) Time series of (a)–(e) variables $D^{(1)}$ (blue) and $D^{(2)}$ (red), and (f)–(j) synchronizability, σ : (a) and (f): $\Delta\mu = 0.0000$, $\beta = 0.0070$, complete synchronization ($\sigma \rightarrow 0$); (b) and (g): $\Delta\mu = 0.0100$, $\beta = 0.0050$, phase synchronization ($\sigma_P = 3$); (c) and (h): $\Delta\mu = 0.0855$, $\beta = 0.0085$, phase synchronization ($\sigma_P = 5$); (d) and (i): $\Delta\mu = 0.0260$, $\beta = 0.0154$, phase synchronization ($\sigma_P = 6$); (e) and (j): $\Delta\mu = 0.0770$, $\beta = 0.0565$, chaos ($\sigma_P \rightarrow \infty$).

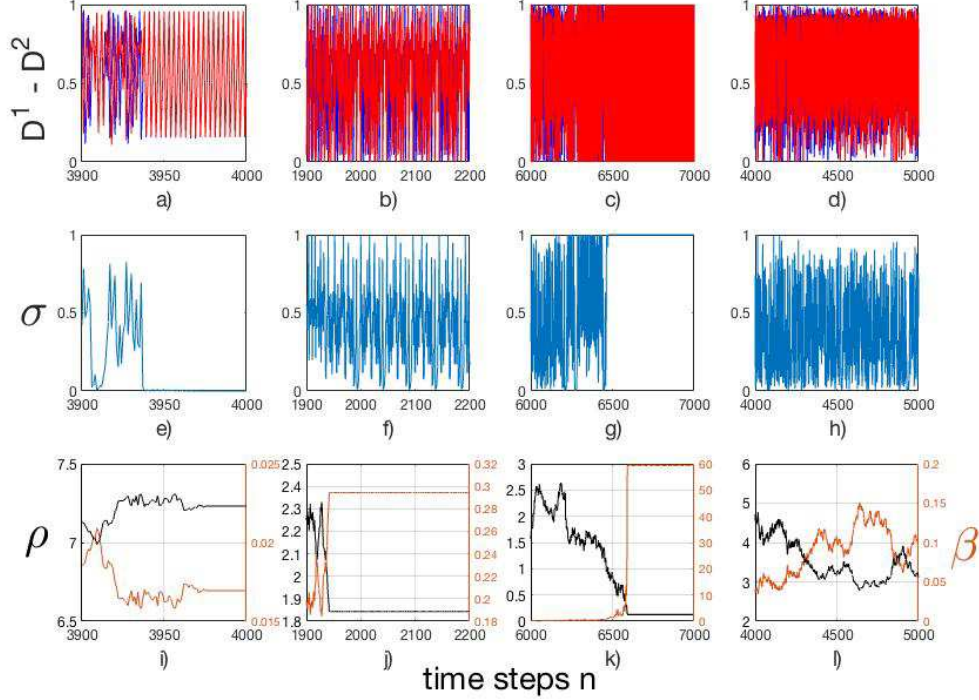


FIG. 7.— (Color online) Time series of, (a)–(d), the dynamical variables $D^{(1)}$ (blue) and $D^{(2)}$ (red); (e)–(h) the synchronizability factor σ ; (i)–(l) the relative distance ρ (black) and coupling strength, β (brown). The first column (a), (e) and (i) illustrates complete synchronization, with initial conditions (i.c.): $\vec{V}_0^{(1)} = (D_0^{(1)}, x_0^{(1)}, y_0^{(1)}, z_0^{(1)}) = (0.150, 5.250, 8.000, 5.250)$; $\vec{V}_0^{(2)} = (D_0^{(2)}, x_0^{(2)}, y_0^{(2)}, z_0^{(2)}) = (0.250, 8.000, 5.250, 8.000)$; $\rho = 1.900$; (b), (f) and (j) show a phase synchrony, with i.c.: $\vec{V}_0^{(1)} = (D_0^{(1)}, x_0^{(1)}, y_0^{(1)}, z_0^{(1)}) = (0.10, 8.25, 5.00, 8.25)$; $\vec{V}_0^{(2)} = (D_0^{(2)}, x_0^{(2)}, y_0^{(2)}, z_0^{(2)}) = (0.250, 5.000, 8.250, 5.000)$; $\rho = 1.900$, with a period $\sigma_P = 48$; (c), (g) and (k) show a anti-synchrony, with i.c.: $\vec{V}_0^{(1)} = (D_0^{(1)}, x_0^{(1)}, y_0^{(1)}, z_0^{(1)}) = (0.100, 5.000, 5.000, 5.000)$; $\vec{V}_0^{(2)} = (D_0^{(2)}, x_0^{(2)}, y_0^{(2)}, z_0^{(2)}) = (0.250, 8.300, 8.756, 8.000)$; $\rho = 0.2$, with a period $\sigma_P = 2$; (d), (h) and (l) show a chaotic situation, with i.c.: $\vec{V}_0^{(1)} = (D_0^{(1)}, x_0^{(1)}, y_0^{(1)}, z_0^{(1)}) = (0.150, 5.250, 8.000, 5.250)$; $\vec{V}_0^{(2)} = (D_0^{(2)}, x_0^{(2)}, y_0^{(2)}, z_0^{(2)}) = (0.250, 8.000, 5.250, 8.000)$; $\rho = 1.900$, with a period $\sigma_P \rightarrow \infty$. All pics with $\mu_1 = \mu_2 = 3.830$

where $d_{\text{threshold}}$, is a threshold distance that ensures non-collision between oscillators, thus avoiding an infinite coupling strength.

3.7. Synchronization Regions

Our system is composed of two coupled logistic maps. To study the synchronization regions in the parameter plane, we determine a correlation between, coupling strength β , parameter mismatch $\Delta\mu$ and σ_n . And the most important and “new” approach: β vs. parameter mismatch $\Delta\mu$, and the σ -periodicities.

$$D_{n+1}^{(1)} = \left(\mu^{(1)} + \frac{\Delta\mu}{2} \right) D_n^{(1)} \left(1 - D_n^{(1)} \right) + \beta \left(D_n^{(2)} - D_n^{(1)} \right)$$

$$D_{n+1}^{(2)} = \left(\mu^{(2)} + \frac{\Delta\mu}{2} \right) D_n^{(2)} \left(1 - D_n^{(2)} \right) + \beta \left(D_n^{(1)} - D_n^{(2)} \right)$$

4. RESULTS

We can characterize the synchronization of the system following the model described in Sect. 3, revealing the synchronizability or synchronization factor σ in terms of the parameters, i.e., $\mu^{(1)} - \mu^{(2)}$, where σ ,

has been computed taking the mean over the last 700 values. The parameters $\mu^{(i)}$, ($i = 1, 2$) where for simplicity, we adopt the notation $\mu^{(i)} = \mu_i$, are defined in the interval $[3, 4]$, regions where the logistic coupled maps can exhibit regular or chaotic behavior, as was reported by Bustos-Espinoza & Ramírez-Ávila (2012). In Fig. 1, we show a three-dimensional insight $\mu_1 - \mu_2 - \sigma$ that represents the surface generated after $n = 10^6$ time steps, and considering a coupling strength, $\beta = 0.0029$. The projection of Fig. 1 onto the plane $\mu_1 - \mu_2$ (the parameter plane) is shown in Fig. 2, where the color code is related to the value of σ . Both from Figs. 1 and 2, it is easy to identify a remarkable point for which σ plummets to zero. This point corresponds to $\mu_1 = \mu_2 = 3.83$. In what it follows, we will consider these values of μ_i as referential ones to describe the dynamical behavior of the (10) coupled maps when the parameter mismatch ($\Delta\mu$) is increased. The computation of the σ values when varying the coupling strength (β) and $\Delta\mu$ results in constructing the phase diagram of the system after an extensive analysis of the periodicities.

4.1. Constant Coupling

In order to find the synchronization regions for the system of two coupled logistic map, we follow the model explained in Sect. 3, i.e., $\beta = \text{const}$ or nonmoving oscillators. We recompute the synchronizability σ using Eq. (10) and introducing the parameter mismatch $\Delta\mu = \mu_1 - \mu_2$, i.e., when both oscillators are identical $\Delta\mu = 0$ or they are nonidentical $\Delta\mu \neq 0$. We chose an ample interval of coupling strength values, β , obtaining a new parameter plane given by β vs. $\Delta\mu$ and depicted in terms of the σ -values shown in Fig. 3, where it is notable the symmetry manifested for the quadratic form of the logistic maps.

To know more about the dynamics of the system, we choose some points inside some regions of Fig. 3 for obtaining the evolution of the dynamical variables, $D^{(i)}$, ($i = 1, 2$), and their corresponding σ_n time series shown in Fig. 4(a)–(e) and Fig. 4(f)–(j) respectively.

From Fig. 4(a) we observe that the signals are completely synchronized, i.e. our quantifier of the phenomenon, σ , goes to zero ($\sigma \rightarrow 0$) as it is shown in Fig. 4(f). In Figs. 4(b)–(d), we can see that the time series are in phase synchronization, whose synchronizability factor oscillates with a well defined period, shown in Figs. 4(g)–(i). Finally, in Figs. 4(e) and (j) the time series exhibit a chaotic behavior and their synchronizability σ oscillates without any specific period. Time series of (a)–(e) variables $D^{(1)}$ (blue) and $D^{(2)}$ (red), and (f)–(j) synchronizability, σ , are: (a) and (f): $\Delta\mu = 0.0000$, $\beta = 0.0064$, *complete synchronization* ($\sigma \rightarrow 0$); (b) and (g): $\Delta\mu = 0.2045$, $\beta = 0.0342$, *phase synchronization* ($\sigma_P = 5$); (c) and (h): $\Delta\mu = 0.0220$, $\beta = 0.0128$, *phase synchronization* ($\sigma_P = 6$); (d) and (i): $\Delta\mu = 0.0695$, $\beta = 0.0128$, *phase synchronization* ($\sigma_P = 10$); (e) and (j): $\Delta\mu = 0.0685$, $\beta = 0.0545$, *chaos* ($\sigma_P \rightarrow \infty$).

4.2. Periodicities

To have a deeper insight of the system's dynamical properties, we analyze the parameter plane by measuring the periods of the synchronizability, σ_P taking the mean over the last 500 values of each σ . With this technique we obtain a new extended parameter plane, β vs. $\Delta\mu$ described in terms of the periodicities σ_P , shown in Fig. 5, where the horizontal color bar represents the main periodicities appearing in the synchronization regions. The extreme cases, complete synchrony and chaos, are defined as that they do not have any periodicity because the synchronizability in these cases remains stable or oscillates chaotically, respectively. Note that the symmetry and the relevant regions of apparent same σ values in Fig. 5. Another interesting issue found in the upper part of Fig. 5, below the orange region with periodicity 3, is the presence of regions with similar shapes to those found by Ramírez-Ávila & Gallas (2011) in the parameter space of the Tinkerbell map.

To test the system we choose some points inside specific regions for evaluating the dynamic variables, $D^{(i)}$, and their corresponding synchronizability σ , as we can see in Fig. 6(a)–(e) and Fig. 6(f)–(j) respectively. The time series of the variables $D^{(1)}$ and $D^{(2)}$

are represented in blue and red respectively. The chosen points $(\Delta\mu, \sigma)$ were: (0.0000, 0.0070), showing *complete synchronization*, i.e. $\sigma \rightarrow 0$; (b) and (g): (0.0100, 0.0050), exhibiting *phase synchronization*, with $\sigma_P = 3$; (c) and (h): (0.0855, 0.0085), also displaying *phase synchronization*, with $\sigma_P = 5$; (d) and (i): (0.0260, 0.0154), also showing *phase synchronization*, with $\sigma_P = 6$; and finally (e) and (j): (0.0770, 0.0565), illustrating *chaotic* behavior, without any specific periodicity. Note the integer sequence of periods: 3, 5, 6, 10, 12, 20, 24, 40, 48, 80, 96,...

4.3. Integer Sequence of Periods

We found the integer sequence of periods: 3, 5, 6, 10, 12, 20, 24, 40, 48, 80, 96, ..., might be described by the recurrent integer sequence relation given by Eq. (11), with a new seed, i.e., $P(1) = 3$ and $P(2) = 5$, different of what was found by Brockhaus (2009). We do not include the extreme cases of complete synchronization and chaos.

$$\begin{aligned} P(n) &= 2P(n-2) \quad (n > 2); \\ P(1) &= 3, \quad P(2) = 5 \end{aligned} \quad (11)$$

4.4. Distance dependence

As we proposed in Sect. 3, synchronization depends on the magnitude of the coupling strength, β , i.e., we can consider a system where the oscillators can move according to Eqs. (8) and (9); that means a permanent change in the spatial positions before they can synchronize. In several cases, movement tends to facilitate synchronization, as was pointed out by Bustos-Espinoza & Ramírez-Ávila (2012). In this work, we study an amplified parameter plane in order to confirm if the movement enhances or not the synchronization. To this end, we study the abstract vector \vec{V} , defined in Eq. (5), i.e., the dynamical variables, $D^{(i)}$, ($i = 1, 2$), the relative distance between oscillators, ρ , altogether with their correspondent coupling strength, $\beta \propto \rho^{-2}$ and the synchronizability factor, σ , the whole as a function of time n . The results are shown in a matrix of graphs shown in Fig. 7, where we can check the time series of the dynamical variables $D^{(1)}$ (blue) and $D^{(2)}$ (red), in Fig. 7(a)–(d); the synchronizability σ in Fig. 7(e)–(h), and the relative distance, ρ (black) and the coupling strength, β (brown) in Fig. 7(i)–(l). Drawing attention to the columns, the first one Figs. 7(a), (e) and (i) describing the situation of complete synchronization, with the initial conditions (i.c.): $\vec{V}_0^{(1)} = (D_0^{(1)}, x_0^{(1)}, y_0^{(1)}, z_0^{(1)}) = (0.15, 5.250, 8.000, 5.250)$; $\vec{V}_0^{(2)} = (D_0^{(2)}, x_0^{(2)}, y_0^{(2)}, z_0^{(2)}) = (0.250, 8.000, 5.250, 8.000)$; a threshold distance, $d_{\text{threshold}} = \rho = 1.900$; (b), (f) and (j) shown a phase synchrony, with i.c.: $\vec{V}_0^{(1)} = (D_0^{(1)}, x_0^{(1)}, y_0^{(1)}, z_0^{(1)}) = (0.10, 8.250, 5.000, 8.250)$; $\vec{V}_0^{(2)} = (D_0^{(2)}, x_0^{(2)}, y_0^{(2)}, z_0^{(2)}) = (0.25, 5.000, 8.250, 5.00)$; with a threshold distance, $\rho = 1.900$, and a periodicity value, $\sigma_P = 48$. In the situation shown in (c), (g) and (k) we decrease the threshold distance, $\rho = 0.2$ in order to get an anti-synchronization, i.e., $D_n^{(1)} + D_n^{(2)} = 1$, with i.c.:

$$\vec{V}_0^{(1)} = (D_0^{(1)}, x_0^{(1)}, y_0^{(1)}, z_0^{(1)}) = (0.10, 5.000, 5.000, 5.00);$$

$$\vec{V}_0^{(2)} = (D_0^{(2)}, x_0^{(2)}, y_0^{(2)}, z_0^{(2)}) = (0.25, 8.300, 8.756, 8.00).$$

In this column the dynamic oscillation goes from 0 to 1 repeating a few times ($n = 118$); and finally, (d), (h) and (l), shown a chaos situation, with i.c.:
 $\vec{V}_0^{(1)} = (D_0^{(1)}, x_0^{(1)}, y_0^{(1)}, z_0^{(1)}) = (0.15, 5.250, 8.000, 5.25);$
 $\vec{V}_0^{(2)} = (D_0^{(2)}, x_0^{(2)}, y_0^{(2)}, z_0^{(2)}) = (0.25, 8.000, 5.250, 8.000);$
 a threshold distance, $\rho = 1.900$, with a periodicity $\sigma_P \rightarrow \infty$. All pics were calculated with $\mu_1 = \mu_2 = 3.830$

5. CONCLUSIONS AND PERSPECTIVES

Using the proposed model and the extended domain of our parameters we get an amplified new synchronization region, where we apply the periodicity technique, reported by Bustos-Espinoza & Ramírez-Ávila (2016), in order to get a new phase diagram. It was possible to identify a natural sequence of integers (periods) that appear on our map, this sequence comes from a bifurcation cascade into the parameter plane, exiting a chaotic window and going to another chaotic region in a system of two coupled logistic maps whose dynamical behavior in terms of their integer periodicities, follows a recurrence relation with a new seed, a different to that found by Brockhaus (2009), who combine the series, $P(n) = 3 \times 2^n$ and $P(n) = 5 \times 2^n$, but without initial term 3 in the first one.

In our study of static and dynamic situations, we find in both cases other types of synchronization besides the complete one, i.e. phase and anti synchronization. The abstract vector, which includes dynamics and spatial positions, enables us to understand in

a deeper way the dynamical aspects related to synchronization in this type of system. Another important result is the confirmation that movement tends to enhance synchronization.

Our comprehensive study on the synchronization of coupled logistic maps using periodicities, allowed us to find synchronization regions with shapes very different to the typical Arnold tongues and with the feature that due to the knowledge of periods, the determination of the so-called winding numbers is done. The huge interval of coupling strength values considered in this work might be essential information in the situation in which the oscillators are moving. This knowledge permits us to know instantaneously whether the oscillators are located in positions allowing synchronization. The method to detect synchronization developed here might be extended to systems with many coupled maps and organized under different topologies similar to those studied by Lind et al. (2004a, 2006). Moreover, our method might also be used for detecting synchronization in other kinds of maps, for instance, in cubic maps exhibiting bistability as those studied by Lind et al. (2004) or multistability as in the case of coupled trios of Rulkov maps considered by Iglesias & Ramírez-Ávila (2019). Finally, it is possible to use other potentials according to the type of movement and interaction between the oscillators, as the Lennard-Jones potential that models soft attractive, and repulsive interactions.

Conflict of interests

Authors declare that there is no conflict of interest with respect to the publication of this document.

REFERENCIAS

- Brockhaus, K. 2009 in The On-Line Encyclopedia of Integer Sequences (A164095), available in <https://oeis.org/A164095>
- Burgoa, K. L., & Nogales, J. A. C. 2001, Revista Boliviana de Física, **7**, 51
- Bustos-Espinoza, R. O. E., & Ramírez-Ávila, G. M. 2016, The European Physical Journal Special Topics, **225**, 2697
- Bustos-Espinoza, R. O. E., & Ramírez-Ávila, G. M. 2012, Revista Boliviana de Física, **22**, 1
- Calderón de la Barca, I., & Ramírez-Ávila, G. M. 2017, Revista Boliviana de Física, **30**, 1
- Chaté, H., & Manneville, P. 1988, Physica D, **32**, 409
- Chua, L. 1993, Journal of Circuits, Systems and Computers, **3**, 93
- Fujisaka, H., & Yamada, T. 1983, Progress of Theoretical Physics, **69**, 32
- Fujiwara, N., Kurths, J., & Díaz-Guilera, A. 2011, Physical Review E, **83**, 025101
- Iglesias, K., & Ramírez-Ávila, G. M. 2019, Revista Boliviana de Física, **34**, 3
- Kaneko, K. 1985, Progress of Theoretical Physics, **74**, 1033
- Kuramoto, Y., & Nishikawa, I. 1987, Journal of Statistical Physics, **49**, 569
- Kocarev, L. (Ed.) 2013, Consensus and Synchronization in Complex Networks (Berlin: Springer)
- García-Cantú, A., Antonopoulos, Ch G., & Basios, V. 2011, Chaos, Solitons & Fractals, **44**, 574
- L'Her, A., Amil, P., Rubido, N., Martí, A. C., & Cabeza, C. 2016, The European Physical Journal B, **89**, 81
- Lind, P. G., Corte-Real, J., & Gallas, J. A. C. 2004, Physical Review E, **69**, 026209
- Lind, P. G., Gallas, J. A. C., & Herrmann, H. J. 2004, Physical Review E, **70**, 056207
- Lind, P. G., Nunes, A., & Gallas, J. A. C. 2004, Physica A, **371**, 100
- Masoller, C., Cavalcante, H. L. D., & Rios Leite, J. 2001, Physical Review E, **64**, 037202
- Masoller, C., & Martí, A. C. 2001, Physical Review Letters, **94**, 134102-4
- Matsumoto, T. 1984, IEEE Transactions on Circuits and Systems, **31**, 1055
- May, R. 1976, Nature, **261**, 459
- Pikovsky, A., Rosenblum, M., & Kurths, J. 2001, Synchronization, A Universal Concept in Nonlinear Sciences (Cambridge: Cambridge University Press)
- Ramírez-Ávila, G. M., Guisset, J. L., & Deneubourg, J. L. 2003, Physica D: Nonlinear Phenomena, **182**, 254
- Ramírez-Ávila, G. M., Guisset, J. L., & Deneubourg, J. L. 2006, Revista Boliviana de Física, **12**, 1
- Ramírez-Ávila, G. M., & Gallas, J. A. C. 2011, Revista Boliviana de Física, **19**, 1
- Schultz, P., Heitzig, J., & Kurths, J. 2014, New Journal of Physics, **16**, 125001
- Subieta-Frias, V. & Ramírez-Ávila, G. M. 2017, Revista Boliviana de Física, **31**, 3
- Sun, H., & Cao, H. 2016, Communications in Nonlinear Science and Numerical Simulation, **40**, 15
- Tang, Y., Mees, A., & Chua, L. 1983, IEEE Transactions on Circuits and Systems, **30**, 620
- Verhulst, P. 1838, Correspondance Mathématique et Physique, **10**, 113
- Yamada, T., & Fujisaka, H. 1983, Progress of Theoretical Physics, **70**, 1240